MULTIBODY DYNAMICS 2003
Jorge A. C. Ambrósio (Ed.)
IDMEC/IST, Lisbon, Portugal, July 1-4 2003

NODAL VS. MODAL REPRESENTATION IN FLEXIBLE MULTIBODY SYSTEM DYNAMICS

Stefan Dietz*, Oskar Wallrapp†, and Simon Wiedemann†

*INTEC GmbH
Argelsrieder Feld 13
D-82234 Wessling, Germany
e-mail: Stefan.Dietz@simpack.de, web page: http://www.simpack.com

†Munich University of Applied Sciences
Lothstrasse 34
D-80335 Munich, Germany
e-mail: Wallrapp@fhm.edu, web page: http://www.fh-muenchen.de/fb06

Keywords: Flexible Multibody Dynamics, Mode Selections, Deployment, Solar Array.

Abstract. *Throughout the past decades a considerable amount of work has been dedicated to the development and application of formalisms to simulate flexible bodies in a multibody system (MBS). The two most common approaches which describe the deformation of a flexible body with respect to their floating frame of reference are the linear finite element formulation and the linear modal approach using global mode shapes. This paper discusses two topics, which are important in the field of flexible body modelling in multibody systems: a) the consideration of quadratic terms in the equations of deformation and b) the presentation of methods for global mode preparation in order to reduce the computer time for dynamic simulations without a significant loss of accuracy regarding the deformations. The proposed methods are applied in two examples, for the deformation of a anti-roll-bar of a car's front suspension and for the simulation of the deployment of a flexible solar array.*

1 Introduction

The multibody system (MBS) theory is applied to the simulation and analysis of flexible mechanical systems. In this methodology, a flexible multibody system is based on the floating frame of reference formulation. Thus, the flexible body motion is a superposition of a large reference motion and small deformations. An approximation is used to describe field of displacements by a linear combination of assumed shape functions with their corresponding time dependent weighting factors. The shape functions may be obtained using the finite element approach *(nodal approach)*, where local polynomial functions are weighted with

nodal deformations or the *modal approach*, where global eigenfunctions or static displacement fields are weighted with modal coordinates. The latter approach reduces the system order but gives rise to the problem of selecting the shape functions. Subsequently, we assume that the strain and displacements are small, but shortening and tilting effects (e.g. of beam structures) due to high loads have to be considered during calculation of the displacement field. The material law is linear.

The multibody system software SIMPACK is based on a modal representation with respect to the floating reference frame. Based on a finite element model provided by finite element software SIMPACK's finite element interface FEMBS generates this modal representation as Standard Input Data (SID). FEMBS connects SIMPACK with the frequently used commercial FEA tools and SIMPACK's finite element program SIMBEAM, which allows the user to model arbitrary, spatial beam structures. The pre-processing generates the SID. They are the mass and stiffness data needed in SIMPACK including geometric stiffness matrices, which prove to be important when buckling or stiffening effects due to large longitudinal loads have to be taken into account [2].

As shown in [1] the linear theory of elasticity is not sufficient when structures experience loads that approach the critic loads for buckling and tilting or when the coupling between spatial bending and torsion has to be considered. In such cases a non-linear beam theory or a non-linear substructure technique is more suitable. In this paper, kinematical displacement computations are based on non-linearities up to quadratic terms. The method is implemented in SIMPACK and all required matrices can be calculated in SIMBEAM. A subset of these matrices can be calculated in commercial finite element software such as ANSYS or NASTRAN.

The advantage of the modal approach is the small number of degrees of freedom, thus reducing the computational burden considerably compared to the nodal approach. The modal method however requires the pre-calculation of the mode shapes to be used (for example by solving eigensystems or static problems) in advance of the simulations. As many authors have shown, the quality of results obtained with the modal approach depends (besides numerical aspects) exclusively on the quality of the mode shapes used in the simulations that is on how accurate the mode shapes can represent the real deformations. Thus, since the actual loads, their frequency range and the deformations of the bodies are usually not known beforehand, the choice of mode shapes is often random (assumed modes), as are the results of such simulations. It is known that even a very small number of proper mode shapes can lead to results close to or equal to those obtained with a FE approach.

This paper discusses methods for a straightforward selection of mode shapes in advance of the simulations and compares results using both, the nodal and the modal approach. This process of mode selection starts with the analysis of the connection of the flexible body with the multibody system and the frequency range of interest. These information are sufficient to set-up the set of modes for analysing the dynamics of a multibody system.

Additionally, the influence of the geometric stiffness matrices and kinematical displacement computation with quadratic terms is studied. The results are compared with

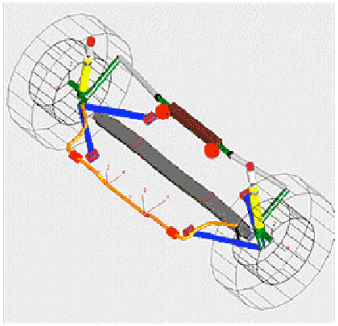

Figure 1: Anti-roll-bar of a car's front suspension

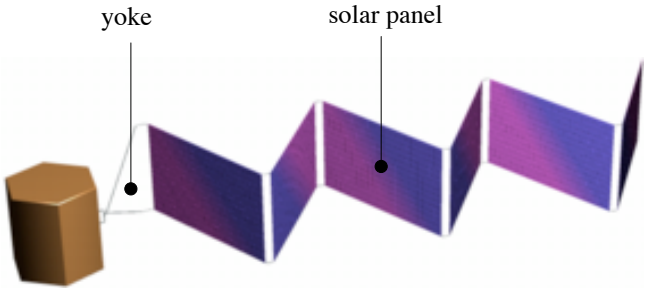

Figure 2: Deployment of a flexible solar array

results obtained using ANSYS and the nonlinear absolute nodal coordinate formulation (ANCF) [3].

The first example of an *anti-roll-bar* of a car's front suspension (Fig. 1) is a spatial beam structure that is modelled by means of SIMBEAM. Static and dynamic load cases are simulated using SIMBEAM and SIMPACK. The second example is a flexible satellite solar array (Fig. 2). The goal of the simulation is to compute the flexible behaviour during deployment. In addition to [4] new methods for mode shape creation are applied to increase accuracy and to reduce the computational burden. The mode shapes of the flexible bodies (yoke and six panels) are created using NASTRAN and FEMBS and the deployment simulation is made using SIMPACK.

2 NOTATION OF THE FLEXIBLE MULTIBODY SYSTEM THEORY

A brief description of the equations of motion of a flexible multibody system as published in many papers [5, 6] is given to explain the notation and to give an overview of the assumptions made for such formulations.

Consider a multibody system of n bodies where the motion is described by a set of position and velocity variables $\mathbf{z}_I^i(t)$ and $\mathbf{z}_{II}^i(t)$, respectively for each body i. A multibody system may now be obtained from the general model of continuum mechanics by formulating three types of constraint equations: (1) definition of the models of bodies (i.e. finite element models, beams, etc.) to be used for a specific analysis; (2) introducing a specific floating frame of reference to describe body deformations; (3) constraints due to joints between the nodes on the bodies. The explicit form of constraints of types 1 and 2 relates the displacement field of all the points of the multibody system to the variables $\mathbf{z}_I^i$ and $\mathbf{z}_{II}^i$. Constraints of type 3 due joints $a = 1, .. n_c$, between bodies i and j can be written implicitly as

$$\mathbf{g}^a(\mathbf{z}_I^i, \mathbf{z}_I^j, t) = \mathbf{0} \tag{1}$$

Formulating all types of constraint equations and applying one of the principles of dynamics, one can generate the system equations in descriptor form or in state space form. An

intermediate result of such a derivation of the equations of motion for a system of n flexible bodies is the virtual power expression due to inertia, internal forces of elasticity and applied body and surface forces

$$\delta P = \sum_{i=1}^{n} \delta \mathbf{z}_{II}^{i\,T} \left(\mathbf{M}^{i}\, \dot{\mathbf{z}}_{II}^{i} + \mathbf{h}_{\square}^{i} + \mathbf{h}_{e}^{i} + \mathbf{h}_{g}^{i} + \mathbf{h}_{f}^{i} + \mathbf{h}_{c}^{i} \right) = 0 . \tag{2}$$

The matrices $\delta \mathbf{z}_{II}^{i}$ are the virtual velocities, belonging to the generalized velocities $\mathbf{z}_{II}^{i}$, $\mathbf{M}^{i}$ and $\mathbf{h}_{c}^{i}$ are the corresponding generalized masses and constraint forces, respectively. $\mathbf{h}_{\square}^{i}$ are generalised inertia forces due to motion of the body reference frame, $\mathbf{h}_{e}^{i}$ represents the internal forces due to deformations, and $\mathbf{h}_{g}^{i}$ and $\mathbf{h}_{f}^{i}$ consider gravitational forces and nodal forces and torques on body i, respectively.

Jourdain's principle states that the virtual power of the constraint forces, result of all types of constraints, is zero. In (2), the virtual power expressions due to constraints of type 1 and 2 do not appear, but the virtual power due to constraints of type 3 is given explicitly. The expression

$$\mathbf{M}^{i}\, \dot{\mathbf{z}}_{II}^{i} = \mathbf{h}_{\square}^{i} + \mathbf{h}_{e}^{i} + \mathbf{h}_{g}^{i} + \mathbf{h}_{f}^{i} + \mathbf{h}_{c}^{i} \tag{3}$$

together with (1) are the equations of motion of a body i, where $\mathbf{h}_{c}^{i}$ are the generalised constraint forces due to joints on body i.

In this formulation the flexible body motion is separated into a motion of a floating frame of reference and small deformations. Summing the products of known shape functions and unknown weighting coefficients, called the modal coordinates, approximates the displacement field due to deformation. Hence, the absolute position $\underline{\square}$ of a point P at physical coordinate $\underline{R}$ on body i at time t is given by the absolute position $\underline{\square}^{i}$ of the body reference frame $\{O^{i}, \underline{\mathbf{e}}^{i}\}$ with respect to the inertia frame $\{O^{I}, \underline{\mathbf{e}}^{I}\}$ and the relative position $\underline{r}(\underline{R})$, see Fig. 3. Here and in all the following, vectors are expressed in coordinates of the body reference frame and are indicated by a bold letter, but the time dependence of variables is not always written.

The absolute position of P is expressed as

$$\square(\mathbf{R}) = \square^{i} + \mathbf{r}(\mathbf{R}) \qquad \text{where} \qquad \mathbf{r}(\mathbf{R}) = \mathbf{R} + \mathbf{u}(\mathbf{R}) , \tag{4}$$

and where $\mathbf{u}(\mathbf{R}, t)$ is the elastic deflection at $\mathbf{R}$.

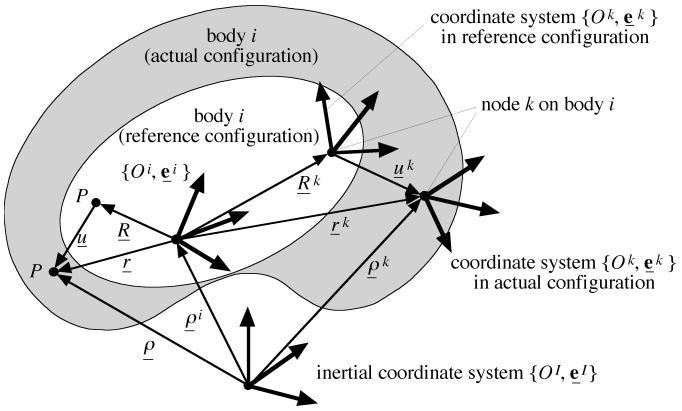

Figure 3: General model of a representative flexible body i.

The absolute orientation of a coordinate system $\{P, \underline{\mathbf{e}}\}$ attached to a section of a body (in case of beam models attached to the beam section at $\underline{R}_1$) or of a frame $\{O^k, \underline{\mathbf{e}}^k\}$ at a node k on body i (Fig. 3) is given by the product of the orientation matrix $\mathbf{A}^i$ of the body reference frame with respect to the inertia frame and the orientation matrix $\Psi(\mathbf{R})$ of the section frame with respect to the body reference frame as

$$\mathbf{A}(\mathbf{R}) = \Psi(\mathbf{R})\,\mathbf{A}^i \quad \text{satisfying} \quad \underline{\mathbf{e}} = \mathbf{A}(\mathbf{R})\,\underline{\mathbf{e}}^I \tag{5}$$

Matrices $\mathbf{A}^i$ and Ψ are parameterised by angles $\Psi^i(t)$ and $\Psi(\mathbf{R}, t)$, respectively.

Linear velocity $\mathbf{v}$ and angular velocities Ω of a body section at point P are derived by differentiation of (4) with respect to time and using the Poisson formula on (5), thus

$$\begin{aligned}
&\mathbf{v}(\mathbf{R}) = \mathbf{v}^i + \Omega^i\,\mathbf{r}(\mathbf{R}) + \dot{\mathbf{r}}(\mathbf{R}) = \mathbf{v}^i - \tilde{\mathbf{r}}(\mathbf{R})\,\Omega^i + \dot{\mathbf{r}}(\mathbf{R}) \\
&\Omega(\mathbf{R}) = \Omega^i + \mathbf{w}(\mathbf{R}) \quad \text{satisfying} \\
&\Omega^i \equiv {}^i\Omega^{iI} = \mathbf{A}^i\,\dot{\mathbf{A}}^{iT}, \;\; \tilde{\mathbf{w}} \equiv {}^i\tilde{\mathbf{w}}^{ki} = \dot{\Psi}^T\Psi, \\
&\text{where} \quad \dot{\mathbf{r}}(\mathbf{R}) = \dot{\mathbf{u}}(\mathbf{R}) \quad \text{and} \quad \mathbf{w} = \mathbf{W}(\Psi)\,\dot{\Psi}
\end{aligned} \tag{6}$$

Note that $\mathbf{v}^i$ and Ω^i are the linear and angular velocities of the reference frame. Variables Ψ^i, $\mathbf{A}^i$, $\mathbf{v}^i$ and Ω^i depend on time t and describe the motion of the reference frame of body i. Variables $\mathbf{r}$, Ψ, $\dot{\mathbf{r}}$, and $\mathbf{w}$ or $\mathbf{u}$, Ψ, $\dot{\mathbf{u}}$, and $\dot{\Psi}$ depend on coordinates $\mathbf{R}$ and time t and represent the deformation of the body. Referring to the specific floating frames of reference such as tangent frame, cord / plane frame, or Tisserand / Buckens frame, $\mathbf{u}$ and Ψ have to satisfy six constraints of reference conditions given in [5].

The deformation variables in (4) to (6) are approximated by known shape functions $\Psi(\mathbf{R})$ and time dependent weighting coefficients or elastic coordinates $\mathbf{q}^i(t)$. In general we can write

$$\mathbf{d}(\mathbf{R},t) = \begin{bmatrix}\mathbf{u}\\ \boldsymbol{\varphi}\end{bmatrix} = \mathbf{d}\Big(\boldsymbol{\Phi}(\mathbf{R}), \mathbf{q}^i(t)\Big),$$
$$\dot{\mathbf{d}}(\mathbf{R},t) = \begin{bmatrix}\dot{\mathbf{u}}\\ \dot{\boldsymbol{\varphi}}\end{bmatrix} = \frac{\partial \mathbf{d}}{\partial \mathbf{q}^i}\,\dot{\mathbf{q}}^i = \boldsymbol{\Phi}(\mathbf{R},\mathbf{q}^i)\,\dot{\mathbf{q}}^i(t) \tag{7}$$

It is assumed that mode shape matrices $\boldsymbol{\Phi}(\mathbf{R})$ or $\boldsymbol{\Phi}(\mathbf{R})$ satisfy both, the constraints of the chosen continuum model (type 1) and the chosen reference frame (type 2). Thus, the elastic coordinates $\mathbf{q}^i$ are independent of these types of constraints.

Using a linear material law but still a nonlinear strain-displacement relation the virtual power of the internal forces defined in (2) are derived by

$$\delta P_i^i = \delta \mathbf{z}_{II}^{i\,T}\ \mathbf{h}_e^i = \int_{V_0^i} \delta\boldsymbol{\varepsilon}^T\ \boldsymbol{\sigma}\ dV = \delta\dot{\mathbf{q}}^{i\,T}\ \mathbf{k}^i, \tag{8}$$

where strain $\boldsymbol{\varepsilon}$, virtual strain velocity $\delta\dot{\boldsymbol{\varepsilon}}$ and stress $\boldsymbol{\sigma}$ are given as

$$\boldsymbol{\varepsilon}(\mathbf{R},t) = \boldsymbol{\varepsilon}(\boldsymbol{\Phi},\mathbf{q}^i),\ \delta\dot{\boldsymbol{\varepsilon}}(\mathbf{R}) = \mathbf{B}(\mathbf{R},\mathbf{q}^i)\,\delta\dot{\mathbf{q}}^i, \quad \mathbf{B} = \frac{\partial \boldsymbol{\varepsilon}}{\partial \mathbf{q}^i}, \tag{9}$$

$$\boldsymbol{\sigma}(\mathbf{R},t) = \mathbf{H}(\mathbf{R})\,\boldsymbol{\varepsilon}(\mathbf{R},t) + \boldsymbol{\sigma}_0(\mathbf{R}) \tag{10}$$

to give the general internal forces of body i as a nonlinear function of $\mathbf{q}^i$

$$\mathbf{k}^i(\mathbf{q}^i) = \int_{V_0^i} \mathbf{B}^T\ \boldsymbol{\sigma}\ dV = \int_{V_0^i} \mathbf{B}^T(\mathbf{R},\mathbf{q}^i)\Big(\mathbf{H}\,\boldsymbol{\varepsilon}(\mathbf{R},\mathbf{q}^i) + \boldsymbol{\sigma}_0\Big)\,dV \tag{11}$$

In (9) to (11), $\mathbf{B}$ is the nonlinear strain matrix, $\mathbf{H}$ is Hooke's matrix, $\boldsymbol{\sigma}_0$ is the matrix of initial stresses and V_0^i is the body volume in the reference configuration.

The equations of motions due to deformations with respect to the reference frame are derived as

$$\mathbf{M}_e^i\ \ddot{\mathbf{q}}^i + \mathbf{D}_e^i\,\dot{\mathbf{q}}^i + \mathbf{k}^i(\mathbf{q}^i) = \boldsymbol{\Phi}^T(\mathbf{R},\mathbf{q}^i)\ \ \mathbf{p}^i(\mathbf{R},t) \tag{12}$$

where $\mathbf{M}_e^i$ is the generalized mass matrix, $\mathbf{D}_e^i$ is a matrix of structural damping and $\mathbf{p}^i$ is the matrix of nodal, volume, and inertia forces and torques. $\mathbf{M}_e^i$ is obtained when introducing a matrix of mass properties $\boldsymbol{\Theta}$ containing density ρ and inertia moments j_1, j_2, j_3 as

$$\mathbf{M}_e^i = \int_{V_0^i} \boldsymbol{\Phi}^T\ \boldsymbol{\Theta}\ \boldsymbol{\Phi}\ dV, \quad \boldsymbol{\Theta} = diag\begin{pmatrix}\rho & \rho & \rho & j_1 & j_2 & j_3\end{pmatrix} \tag{13}$$

All matrices of a flexible body are saved in the SID file where the space dependent integrals are computed in pre-processors such as SIMBEAM or FEMBS together with FE-software.

Finally, the position, velocity and virtual velocity variables of body *i* introduced in (1) to (3) are given as

$$\mathbf{z}_I^i = \begin{bmatrix} \boldsymbol{\Phi}^i \\ \boldsymbol{\Omega}^i \\ \mathbf{q}^i \end{bmatrix}, \qquad \mathbf{z}_{II}^i = \begin{bmatrix} \mathbf{v}^i \\ \boldsymbol{\omega}^i \\ \dot{\mathbf{q}}^i \end{bmatrix}, \qquad \delta\mathbf{z}_{II}^i = \begin{bmatrix} \delta\mathbf{v}^i \\ \delta\boldsymbol{\omega}^i \\ \delta\dot{\mathbf{q}}^i \end{bmatrix} \tag{14}$$

containing the variables of the reference motion and the elastic coordinates of deformation. All other matrices are given in [5, 6].

3 APPROXIMATION MODELS FOR THE DEFORMATION FIELD

Ever since multibody programs have come into existence, various models to approximate the displacement field due to deformations have been discussed, see e.g. [7]. In this report six models are discussed that are briefly described as follows:

(A) Finite element discretisation where the deformation is linearly approximated by an interpolation matrix, nodal coordinates and linear strain and stress relations.
(B) Extension of model (A) by consideration of initial stresses and their linear terms in the nodal coordinates, the so-called geometric stiffness matrix.
(C) Finite element discretisation where the deformation is quadratically approximated by the interpolation matrix, nodal coordinates, linear strain and stress relations and initial stresses.
(D) Reduction of the computational burden in MBS dynamical simulations using the modal approach. Model (C) is reduced to a matrix of mode shapes taken from an eigenvalue or a static analysis.
(E) The mode shapes taken for model (D) are selected using participation factors [4].
(F) The mode shapes taken for model (D) are selected using an algorithmic strategy.

For comparison of these models, results are partly taken from a nonlinear finite element theory – here the absolute nodal coordinate formulation (ANCF) [3] and ANSYS. The six models are described in detail next.

3.1 Model (A) – linear FE-formulation

The simplest model is a linear expression of the deformation field in (7). Thus, the deformation field of an element *e* at all local element points **x** is described by the interpolation matrix $\mathbf{N}^e(\mathbf{x})$ and nodal element coordinates $\mathbf{z}^e(t)$. One finds the following relations for the deformation, strain $\boldsymbol{\varepsilon}$ and stress $\boldsymbol{\sigma}$ of element *e*

$$\mathbf{d}^e(\mathbf{R},t) = \mathbf{N}^e(\mathbf{x})\,\mathbf{z}^e(t), \quad \dot{\mathbf{d}}^e(\mathbf{R},t) = \mathbf{N}^e(\mathbf{x})\,\dot{\mathbf{z}}^e(t)\,, \tag{15}$$

$$\begin{aligned} \boldsymbol{\varepsilon}^e(\mathbf{x},t) &= \mathbf{B}_L^e(\mathbf{x})\,\mathbf{z}^e(t)\,, \quad \delta\boldsymbol{\varepsilon} = \mathbf{B}_L^e\,\delta\dot{\mathbf{z}}^e\,, \\ \boldsymbol{\sigma}^e(\mathbf{x},t) &= \mathbf{H}^e(\mathbf{x})\,\boldsymbol{\varepsilon}^e(\mathbf{x},t) \end{aligned} \tag{16}$$

where $\mathbf{x} = \mathbf{R} \sqcap \mathbf{R}^e$ and $\mathbf{R}^e$ is the position vector of the local element frame, $\mathbf{B}_L^e$ is the linear strain and $\mathbf{H}^e$ the linear Hooke matrix of an element e. The motion of all elements can be written by all global nodes forming the nodal coordinate vector $\mathbf{z}_F$ of the unsupported finite element (FE) structure. Finally, a nodal state vector $\mathbf{q}_F$ of the supported structure embedded into the MBS floating frame of reference is introduced, which in accordance to (7) yields

$$\begin{aligned} &\mathbf{q}^i \equiv \mathbf{q}_F, \quad \mathbf{z}^e = \mathbf{T}^e\, \mathbf{z}_F = \mathbf{T}^e\, \overline{\mathbf{T}}\, \mathbf{q}^i \quad \text{and} \quad \mathbf{d} = \square\, \mathbf{q}^i \\ &\text{where } \square(\mathbf{R}) \equiv \square_L = \mathbf{N}^e(\mathbf{x})\, \mathbf{T}^e\, \overline{\mathbf{T}} \end{aligned} \tag{17}$$

is the linear mode shape matrix. From (15) and (16) one derives the internal forces and the mass matrix as given in (11) to (13)

$$\begin{aligned} &\mathbf{k}^i(\mathbf{q}^i) = \mathbf{K}_e^i\, \mathbf{q}^i, \quad \mathbf{K}_e^i = \overline{\mathbf{T}}^T \sum_e \left(\mathbf{T}^{eT}\, \mathbf{K}^e\, \mathbf{T}^e\right) \overline{\mathbf{T}}, \\ &\mathbf{K}^e = \int_{V_0^e} \mathbf{B}_L^{eT}\, \mathbf{H}^e\, \mathbf{B}_L^e\, dV^e \end{aligned} \tag{18}$$

$$\mathbf{M}_e^i = \overline{\mathbf{T}}^T \sum_e \left(\mathbf{T}^{eT}\, \mathbf{M}^e\, \mathbf{T}^e\right) \overline{\mathbf{T}}, \quad \mathbf{M}^e = \int_{V_0^e} \mathbf{N}^{eT}\, \square^e\, \mathbf{N}^e\, dV^e \tag{19}$$

$\mathbf{K}^e$ and $\mathbf{M}^e$ respectively are the element stiffness and mass matrices.

For various models of finite elements, interpolation matrices and their stiffness and mass matrices are given in standard FE books. Model (A) is only useful for small elastic deformations. The loads should be small compared to critical loads, for example for buckling and tilting.

3.2 Model (B) – Linear FE Formulation and Geometric Stiffness Matrix

Model (A) is extended by initial stresses $\square_0$ as shown in (10) and a bilinear term in the virtual strain velocity (9). This bilinear term may be derived by a geometrically nonlinear theory, for example for beam [6] and plate models. With the interpolation matrix given for model (A), one finds instead of (16) and (18)

$$\square^e = \mathbf{B}_L^e\, \mathbf{z}^e, \quad \square\square_{\square} = \left(\mathbf{B}_{L\square}^e + \mathbf{z}^{eT}\, \mathbf{B}_{Q\square}^e\right) \square\dot{\mathbf{z}}^e, \quad \square^e = \mathbf{H}^e\, \square^e + \square_o^e \tag{20}$$

$$\mathbf{k}^i(\mathbf{q}^i) = \left(\mathbf{K}_e^i + \mathbf{K}_{\text{geo}}^i\right)\mathbf{q}^i, \quad \mathbf{K}_{\text{geo}}^i = \overline{\mathbf{T}}^T \sum_e \left(\mathbf{T}^{eT}\, \mathbf{K}_{\text{geo}}^e\, \mathbf{T}^e\right) \overline{\mathbf{T}}. \tag{21}$$

In (20) subscript $\square$ depends on the strain variables of a FE model. Matrix $\mathbf{K}_{\text{geo}}^i$ is the geometric stiffness matrix. The element matrix $\mathbf{K}_{\text{geo}}^e$ leads to the specific initial element stresses $\square_o^e$ that are caused by initial loads on FE structures.

Applying the linear theory of elasticity, the actual geometric stiffness matrix of an element can be expressed as a superposition of single load cases L_j on body i and unit geometric

stiffness matrices $\widehat{\mathbf{K}}^{e}_{\mathrm{geo\,j}}$ that are pre-calculated for unit loads. This gives unit stresses σ^{e}_{oj}, see e.g. [2],

$$\mathbf{K}^{e}_{\mathrm{geo}} = \sum_{j} \widehat{\mathbf{K}}^{e}_{\mathrm{geo}\,j}\, L_j\,, \quad \widehat{\mathbf{K}}^{e}_{\mathrm{geo}\,j} = \sum_{\sigma} \int_{V_0^e} \mathbf{B}^{eT}_{Q\sigma}\, \sigma^{e}_{0\sigma\, j}\, dV^{e}\,. \tag{22}$$

For the deformations and the mass matrix, Eqs. (15) and (19) are still applied.

Model (B) allows to calculate the critical buckling and tilting load for beam structures and to take other stiffening effects into account, for example on rotating structures. On the other hand, it should be noted that the model does not compute nonlinear displacements such as the shortening of a beam when bent.

3.3 Model (C) – Quadratic Formulation of Deformations

Applying nonlinear theory, for example for a beam element, the Cartesian deformation variables **d** contain quadratic terms and are expressed by integrals of the beam deformations such as longitudinal strain ε and the curvatures for two bending direction and torsion. The strain relation (20) is still valid, but for $\mathbf{d} = (d_\delta)$ instead of (15) and (17) one writes with $\mathbf{N}^e \equiv \mathbf{N}^e_L = \left(\mathbf{N}^e_{L\delta}\right), \delta = 1, \ldots 6,$

$$\begin{aligned} d_\delta(\mathbf{x}) &= \mathbf{N}^e_{L\delta}(\mathbf{x})\, \mathbf{z}^e + \tfrac{1}{2}\mathbf{z}^{eT}\, \mathbf{N}^e_{Q\delta}(\mathbf{x})\, \mathbf{z}^e \quad \text{and} \\ d_\delta(\mathbf{R}) &= \Gamma_{L\delta}(\mathbf{R})\, \mathbf{q}^i + \tfrac{1}{2}\mathbf{q}^{iT}\, \Gamma_{Q\delta}(\mathbf{R})\, \mathbf{q}^i\,, \quad \delta = 1,\ldots 6 \end{aligned} \tag{23}$$

$\mathbf{N}^e_{Q\delta}$ is a 6×6 shape function matrix of the quadratic expansion and therefore $\Gamma_{Q\delta}$ is a $n_q \times n_q$ matrix given as

$$\Gamma_{Q\delta}(\mathbf{R}) = \overline{\mathbf{T}}^T \sum_{e} \left(\mathbf{T}^{eT}\, \mathbf{N}^e_{Q\delta}(\mathbf{x})\, \mathbf{T}^e\right) \overline{\mathbf{T}}\,. \tag{24}$$

If the longitudinal stress and the bending moment of a beam element is constant with respect to the central axis *x*, then matrices $\mathbf{N}^e_{Q\delta}$ at node *k* are equivalent to the negative values of the unit geometric stiffness matrices $\widehat{\mathbf{K}}^{e}_{\mathrm{geo}\,j}$, where *j* denotes the load case at node *k* in direction δ. More details are given in [1].

Model (C) gives better results than models (A) and (B) if the actual loads approach the critical loads for buckling or tilting or if three dimensional bending and torsion motions of beam elements are analysed. This model is implemented in SIMPACK where the matrices are pre-calculated in SIMBEAM for 3D-beam structures.

3.4 Model (D) – Modal Transformation

The modal approximation is applied. The deformation of the FE structure of a body *i* is given by (12) where damping is neglected and internal forces are incorporated by a simple stiffness matrix as given in (18). This leads to

$$\mathbf{M}_e^i\,\ddot{\mathbf{q}}_F + \mathbf{K}_e^i\,\mathbf{q}_F = \square\,\square_L^T\,\mathbf{p}^i\,, \tag{25}$$

where $\mathbf{q}_F$ is the vector of nodal coordinates of the supported FE structure. The length n_{qF} of $\mathbf{q}_F$ is in general very large.

With (25) eigenvectors and static displacement fields due to specific load cases (static modes) can be created to give a small number (n_q) of mode shapes that are taken into account in the dynamic MBS simulation. The selected mode shapes form the mode matrix $\mathbf{S}_e$ with dimensions n_{qF} times n_q. This yields the new mass, stiffness (modal) and mode shape matrices as

$$\begin{aligned} &\mathbf{q}_F = \mathbf{S}_e\,\mathbf{q}^i \quad \text{and} \\ &\mathbf{M}_e^i := \mathbf{S}_e^T\,\mathbf{M}_e^i\,\mathbf{S}_e\,, \quad \mathbf{K}_e^i := \mathbf{S}_e^T\,\mathbf{K}_e^i\,\mathbf{S}_e\,, \quad \square := \square\,\mathbf{S}_e \end{aligned} \tag{26}$$

respectively, with the reduced dimension n_q to approximately describe the deformation of the flexible body as shown in (12). It should be noted that for model (B) also the geometric stiffness matrix $\mathbf{K}_{\text{geo}}^i$ and for model (C) the quadratic mode shape matrices $\square_{Q\square}$ have to be transformed to modal form. If all modes shapes are orthogonal the modal mass matrix can be scaled to give an identity matrix.

In general, the lower eigenmodes are more important than the higher frequency modes, and static modes increase the accuracy of the modal approximation, see e. g. [5, 9].

3.5 Model (E) – Mode Selection Using Participation Factors

As proposed in [4], accounting for the joints and loads acting on a body during MBS simulations the selection of mode shapes can be done using pre-calculated participation factors. First, a large number of eigenmodes and static modes and the corresponding modal equations as shown in model (D) are created. Second, loads such as nodal and inertial forces or torques are assumed or estimated. Third, a simple static analysis of this system gives deformations at interesting points of the body that are weighted with the used mode shapes to give the (participation) factors. Scaled factors smaller than say 0.01 mean that the share of the corresponding mode shape in the overall deformation is less than 1 % and may be neglected. The remaining modes are taken into account for time simulations.

It is noted that the participation factors are computed for only one situation or point in time and have to be computed for each individual force and joint configuration. However, when using the method to save computer time the factors would be computed for the most interesting force and joint configurations to give good results for these critical points in time.

3.6 Model (F) – Straightforward Mode Selection

Considering the free-body diagram (see Fig. 4 b) of a flexible body shows the following fact: The interaction of the flexible body with its surrounding multibody system may be described by those loads which act in the connections between the flexible body and the

multibody system. These connections are force elements, constraints and the joint, which are attached to the flexible body and the loads acting within these connections

$$\mathbf{p}(\mathbf{R},t) = \sum_{k=1}^{m} \mathbf{p}_k \, q_k(t) \tag{27}$$

can be described by a linear combination of unit loads $\mathbf{p}_k$ with their time dependent weighting factors $q_k(t)$. The number m of unit loads is determined by the number of connections and the number of dimensions of a connection. The next step is to approximate the particular solution of (25)

$$\mathbf{d}^p(\mathbf{R},t) = \mathbf{f}(\mathbf{p}(\mathbf{R},t)), \tag{28}$$

which will be used for the calculation of multibody dynamics and which has therefore to be a modal approximation

$$\mathbf{d}^p(\mathbf{R},t) = \sum_{k=1}^{m} \Phi_k^p(\mathbf{R}) q_k(t), \tag{29}$$

where the $\Phi_k^p(\mathbf{R})$ are referred to as particular mode shapes and the $q_k(t)$ are denoted as their corresponding modal coordinates. Based on a linear description of the flexible body, for example a finite element model, a particular mode shape $\Phi_k^p(\mathbf{R})$ has to be calculated for its corresponding unit load $\mathbf{p}_k$. Regarding the equations of a linear finite element model the most general formulation of particular modes is the *frequency response mode* (frm)

$$\left(\mathbf{K}_e^i - \Omega_0^2 \mathbf{M}_e^i\right) \Phi_k^p = \mathbf{p}_k, \tag{30}$$

which depends on the unit load $\mathbf{p}_k$ harmonically acting on its corresponding attachment point with the excitation frequency Ω_0. Further approximations of the particular solution in modal form are static modes and inertia relief modes. Note that the static mode approach can be derived from the frequency response by setting the excitation frequency to zero. For decreasing main frequencies the frequency response passes into the inertia relief approach. The set of frequency response modes is the exact particular solution if the forces harmonically act with the excitation frequency on the structure. To improve the approximation within a user-defined frequency range

$$0 < \Omega < \Omega_a$$

the set of frm is extended by eigenmodes (em). The question which eigenmodes should be used to extend the frm is subsequently answered in the step-by-step recipe. The combination of eigenmodes Φ_j^h and frm Φ_k^p is an approximation of the general solution for the deformation of the flexible body. The process is continued by the orthogonalisation of the mode set. In the case of FEMBS this means to orthogonalise and normalise the frm

$$\Psi_k^p \quad \underset{\text{orthogonalisation and normalisation}}{\Rightarrow} \quad \bar{\Psi}_k^p \tag{31}$$

in order to meet the orthogonality conditions

$$\Psi_j^{hT}\mathbf{M}_e^i\Psi_k^h = \begin{cases} 1 & \text{for} \quad j=k \\ 0 & \text{for} \quad j\neq k \end{cases} \qquad \Psi_j^{hT}\mathbf{K}_e^i\Psi_k^h = \begin{cases} \omega_j & \text{for} \quad j=k \\ 0 & \text{for} \quad j\neq k \end{cases},$$

$$\bar{\Psi}_j^{pT}\mathbf{M}_e^i\bar{\Psi}_k^p = \begin{cases} 1 & \text{for} \quad j=k \\ 0 & \text{for} \quad j\neq k \end{cases} \qquad \bar{\Psi}_j^{pT}\mathbf{K}_e^i\bar{\Psi}_k^p = \begin{cases} \bar{\omega}_k & \text{for} \quad j=k \\ 0 & \text{for} \quad j\neq k \end{cases}, \tag{32}$$

$$\Psi_j^{hT}\mathbf{M}_e^i\bar{\Psi}_k^p = 0 \qquad \Psi_j^{hT}\mathbf{K}_e^i\bar{\Psi}_k^p = 0.$$

Since the frequencies of $\bar{\omega}_k$ are generally greater than the eigenfrequencies ω_j frm may introduce high frequencies into the multibody system, slowing down SIMPACK's time integration. Moreover, frm corresponding to high frequencies have no significant contributions to the deformation. Therefore, FEMBS allows the user to specify a maximum frequency ω_{max} to deselect frm $\bar{\mathbf{u}}_k^p$ that meet inequation $\bar{\omega}_k > \omega_{max}$. During the orthogonalisation FEMBS can automatically detect and deselect linear dependent modes. Consider the example of a stabilizer bar as shown in Figure 4. In this case the mode selection procedure can be summarized as follows:

Step 1: Analyse the connections of the flexible body: Since the connections of the anti-roll-bar (bushings and spherical constraints) do not transmit moments the unit loads are given by the forces $\mathbf{p}_1$ to $\mathbf{p}_{12}$.

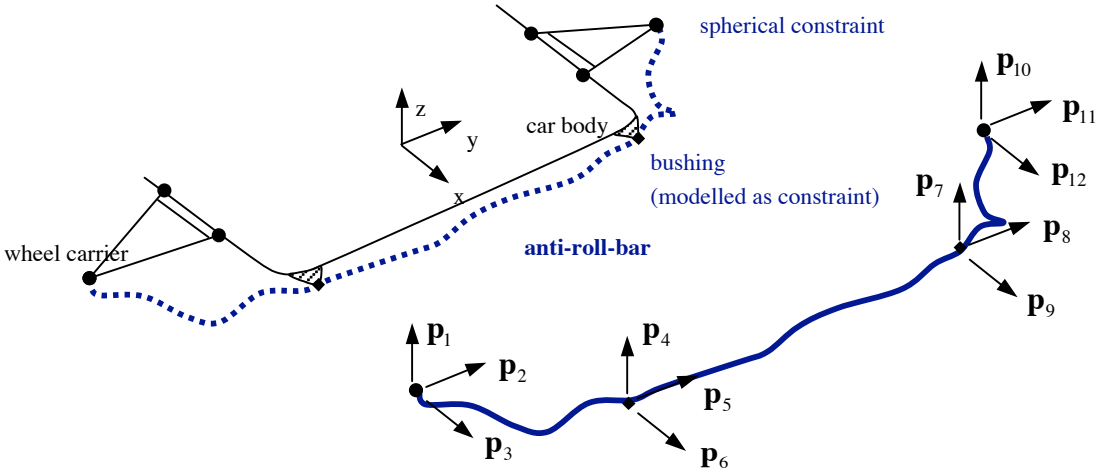

Figure 4: a) MBS model of the anti-roll-bar. b) free body diagram of the anti-roll-bar. See also Fig. 6.

Step 2: Equation (30) shows, that the frequency response will converge towards the first eigenmode if the excitation frequency Ω_0 approaches the first eigenfrequency ω_1 of the structure. Conversely, in the case of excitation frequencies that converge towards zero the frequency response increasingly becomes similar to a linear combination of rigid body modes. Both, neither the first eigenmode nor the rigid body solution contributes new information to the modal approach. Thus, set the excitation frequency for the calculation of the frm to the half of the first eigenfrequency of the structure $\Omega_0 = 1/2\,\omega_1$.

Step 3: Calculate the frm Φ_1^p to Φ_{12}^p for the unit loads $\mathbf{p}_1$ to $\mathbf{p}_{12}$.

Step 4: Define the maximum frequency of interest Ω_a.

Step 5: Calculate and select all eigenmodes, which make a significant contribution to the deformation. Select eigenmodes, which correspond to frequencies within the interval $0 \le \omega_j \le 2.0\,\Omega_a$ as proposed in[10]. A criterion for an alghoritmic selection of eigenmodes in combination with frm is discussed in[8]. This method is similar to the mode selection by contribution factors. The difference is that the method proposed in [8] is based on unit loads, whereas the selection by contribution factors as proposed here and in [4] uses information about loads which were for example calculated by means of a comparable multibody system with rigid bodies instead of flexible bodies. The advantage of the method proposed in [8] is its applicability to dynamic loads and therefore its capability to calculate contribution factors, which consider the free oscillations of a structure as well. Thus, a promising approach seems to be a combination of both methods.

Step 6: To deselect stiff frm after the orthogonalisation has been performed assume unit loads in the frequency range. Their modal contribution at the upper limit of the frequency range Ω_a is given by

$$\bar{q}_k = \frac{1}{\sqrt{\left(\omega_k^2 - \Omega_a^2\right) + 4\omega^2\Omega_a^2}} \,. \tag{33}$$

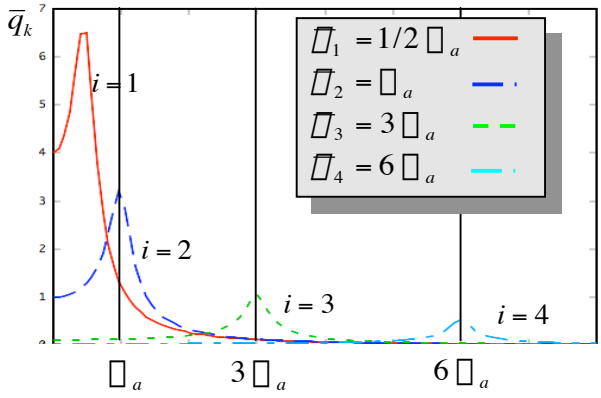

Figure 5: The modal contribution $\bar{q}_k$ of the frm $\bar{\Phi}_4^p$ in the frequency domain. Compare the modal contributions at the upper limit of the frequency range of interest Ω_a

Consider for example the stiff frm $\overline{\square}_4^p$ in Figure 5 with its resonance frequency of $\overline{\square}_4 = 6\square_a$. Its modal contribution within the frequency range of interest $0 < \square < \square_a$ is negligible. Depending on the accuracy requirements of the current application equation (33) can provide assistance with the definition of the maximum frequency. In the example discussed in Fig. 5 the choice $\square_{\max} = 6\square_a$ will be sufficient. frm whose frequency is within the frequency range of interest have to be considered in the MBS-model, see frm $\overline{\square}_1^p$ with the frequency of $\overline{\square}_1$ in Fig. 5. The mode matrix $\mathbf{S}_e$ consists of eigenmodes and frequency response modes and has the dimensions n_{qF} times n_q. The modal transformation is done as described for model (D).

4 SIMULATIONS OF A ANTI-ROLL-BAR

The models for the approximation of the deformation field of a flexible body within a MBS are tested first on a anti-roll-bar of a car front suspension, see Fig. 1. The spatial curved linkage as shown in Fig. 6 is modelled by a 3D beam mesh using 20 nodes for the physical points and an additional node k = 21 for the body reference frame. The mesh has 19 beam elements, thus the mesh leads to a polygon curve of the beam's central line. The number of DOF's of the unsupported structure is n_F = 120, the number of DOF's of the constrained anti-roll-bar is n_q^i = 114. The cross section area of linkage is like a circle with diameter 0.019 m, the material is steel. In Fig. 7 the first two eigenmodes of the unsupported linkage are plotted, using the Buckens frame of reference. The values of the first ten eigenfrequencies are 45.0, 96.7, 113.0, 118.2, 202.4, 286.1, 335.9, 367.9, 430.5 and 521.6 Hz. To discuss the described approximations for deformations, the linkage is constrained at various nodes and loaded by a spatial force **F** and torque **L** at node 20, thus $\mathbf{p}^{20} = (F_x\ F_y\ F_z\ L_x\ L_y\ L_z)^T$. The specific load cases are listed in Table 1.

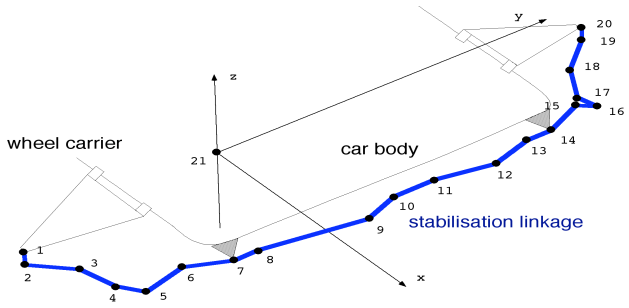

Figure 6: FE-mesh of the anti-roll-bar.

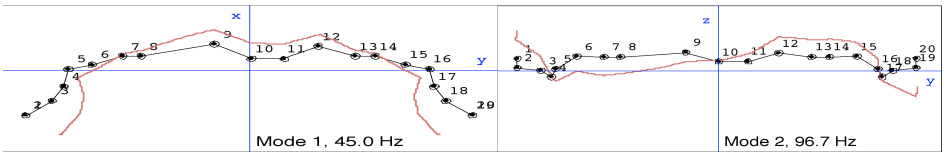

Figure 7: First two eigenmodes (colored lines) of the unsupported linkage.

Load Case	Suspension	Forces at node 20	Torques at node 20
1	clamped at node 1	30, 30, 30 N	0, 0, 0 Nm
2	see 1	100, 100, 100 N	0, 0, 0 Nm
3	*x* at node 1 *x, y, z* at node 7 *x, z* at node 14	0, 0, -1000 N	0, 0, 0 Nm
4	see 3	0, 0, $1000 \cdot \sin(2\pi t)$	0, 0, 0 Nm

Table 1 Load cases for simulations of the anti-roll-bar

4.1 Linear vs. quadratic approximation

To discuss the effects of a quadratic approximation field of the deformation, the linkage is analysed for load cases 1, 2 and 3. For load case 3 the deformed and undeformed linkage are plotted in Fig. 8. Table 2 lists the results of the displacements at node 20, $\mathbf{d}^{20} = (u_x\ u_y\ u_z\ \varphi_x\ \varphi_y\ \varphi_z)^T$ Here the results obtained with the ANCF method serves as the reference solution with 360 DOF's. For comparison, nonlinear ANSYS results of a model with 600 DOF's are also given in Table 2. For the three load cases, the error of the linear model (A) for the displacement u_y is very large. With a growing force (compare case 1 and case 2) also other displacements show errors larger than 3 %. Model (C) dramatically reduces the errors for load case 2 from 33 % to 3.5 %. This implies that the quadratic approximation of the deformation field is a powerful model to describe deformations far beyond the linear case. However, for load case 3 the linkage is largely deformed due to the quadratic formulation, see Fig. 6.

Load Case	Model of approxim.	Displacements / Error in % at node 20					
		u_x mm	u_y mm	u_z mm	φ_x rad	φ_y rad	φ_z rad
1	ANCF	16.119	3.3638	14.771	0.01768	0.00745	-0.0231
	(A)	1	9	1	1	1	1
	(B)	-1	8	0	0	1	0
	(C)	0	1	0	0	-1	0
2	ANCF	53.034	9.1563	47.936	0.05726	0.02428	-0.0753
	ANSYS	53.002	9.1400	47.901	0.05731	0.02432	-0.0754
	(A)	2	33	4	4	3	3
	(B)	-2	30	2	2	2	1
	(C)	0	4	1	1	3	1
3	ANSYS	4.9446	-1.3406	-51.328	-0.0466	-0.2123	0.0093
	(A)	-83	-186	44	42	44	-124
	(B)	-100	-178	4	-3	9	-134
	(C)	-31	52	5	-2	8	-74

Table 2 Deformation of the anti-roll-bar at node 20 for various load cases.
For models (A) to (C) the errors in % are given with respect to ANCF or ANSYS results.

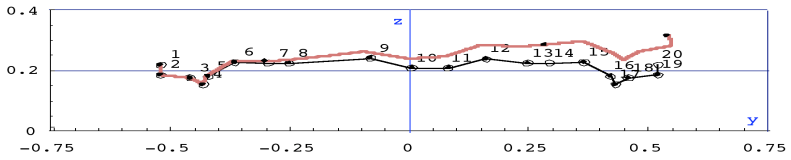

Figure 8: Deformation of the linkage (coloured line, scaled by factor 2) for load cases 3.

4.2 Nodal vs. modal approximation and mode selection

In the following simulations, the modal approximation with a modal reduction is applied. With the modelling options in SIMBEAM and SIMPACK, eigenmodes of the unsupported linkage with a Buckens frame of reference are prepared. It should be noted that for the modal formulation the linkage suspension (six constraints) has to satisfy (1). The six coordinates of the reference frame must be included in the equations of motion (3), together with six Lagrange multipliers representing the constraints. The number of DOF's is thus n_q + 12. For all models a linear theory of deformation is applied, but body reference motions are computed non linearly in SIMPACK. Besides a simple truncation of higher eigenmodes, a mode selection using participation factors as described for model (E) is applied. For load case 2 a graph of factors is plotted in Fig. 9. In the fist case, these15 eigenmodes are selected: 1, 2, 3, 4, 5, 6, 8, 9, 10, 13, 14, 18, 22, 24 and 27. A second set of modes is prepared for factors larger than 0.01, giving a set of 25 modes. To increase the accuracy of the results, two sets of frequency response modes for an excitation frequency of 20 Hz with forces at nodes 1 and 20 for load case 2 and at nodes 1, 7, 14 and 20 for load cases 3 and 4 are prepared, in addition to a few number of eigenmodes. The simulation results are listed in Table 3. To test the mode selection for dynamical models, a harmonic load function (load case 4) is applied. Figure 8 shows the computed displacements u_y and $u_z\,(t)$. Since the linkage is a 3-dimensional structure, loads at node 20 excite all bending and torsion modes.

Thus only a wide range of eigenmodes can describe the deformation of the body correctly, as shown by the participation factors in Fig. 9. It is seen that modes 7 and 11 are not important for this load case, whereas modes 24 and 27 are. A mode selection using participation factors reduces for load case 2 the error from 46 % to 20 % at maximum with respect to the nonlinear results. This mode set needs 100 times less CPU time for load case 3 than the full model with 114 modes while the displacements are similar, see Fig. 10. A set with 9 modes allows for main deformations but cannot correctly represent y-motion. Table 3 and Fig. 10 also show that even using only 3 eigenmodes together with 12 frequency response gives results in close agreement to the reference of the full model.

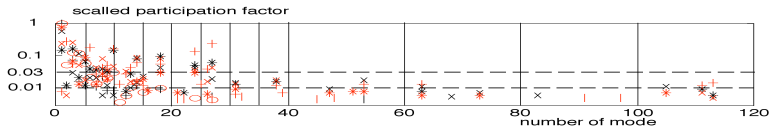

Figure 9: Participation factors of eigen modes calculated for load case 2. Figures lower than 0.03 mean that the share of the corresponding mode in the total (static) deformation is less than 3 %.

Load Case	Model of approxim.	Displacements at node 20 / Error in %					
		u_x mm	u_y mm	u_z mm	φ_x rad	φ_y rad	φ_z rad
2	ANSYS	53.034	9.1563	47.936	0.0573	0.02428	-0.0754
	all 114 em	1	2	3	3	13	2
	first 10 em	-27	24	-39	-32	-40	-17
	first 15 em	-22	18	-27	-19	-46	-13
	15 em-pf	-20	17	-23	-16	-20	-13
	3em+12frm	2	2	4	5	-11	2
3	ANSYS	4.9446	-1.3406	-51.328	-0.0466	-0.2123	0.0093
	all 114 em	-9	-57	0	0	4	-89
	15 em-pf	-9	-54	0	2	3	-83
	3em+12frm	-9	-57	0	0	4	-89

Table 3 Deformation of the linkage. The errors are given with respect to ANSYS results.
em = eigenmodes, pf = selected using participation factors, frm = frequency response modes.

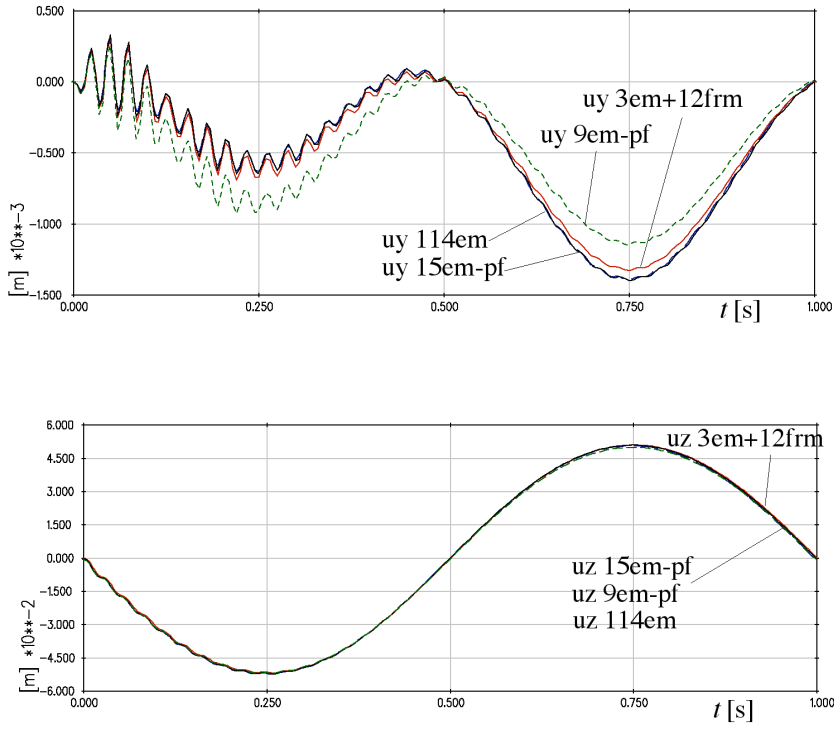

Figure 10: Displacments u_x and u_z (t) at node 20 for load case 5.
em = eigenmodes, pf = selected using participation factors, frm = frequency response modes.

5 SIMULATION OF THE DEPLOYMENT OF A SOLAR ARRAY

Due to the complexity of this model time simulations over 500 s using nodal coordinates to serve as a reference for the true deformations or their best approximations can not be made in a sensible amount of time. Consequently, only a modal representation of the deformation of the flexible bodies can be applied.

In reality, the deployment of the solar array basically takes place in three steps, see Fig. 11 and [4]. In the first step some fixations are released and the deployment springs with a constant torque start working on the yoke and panels, trying to move them. However, since all panels and the yoke are connected via flexible closed cable loops and since the yoke cannot move due to a motor gear unit not activated yet, the springs drive the bodies versus the cables, starting a damped oscillation. This is called jump-out. The second step is the activation of the motor gear unit after 250 seconds, which slowly and smoothly turns the yoke and thus all connected panels. The last step is the final deactivation of the motor gear unit and the activation of lock mechanisms when the array is completely deployed after about 360 seconds.

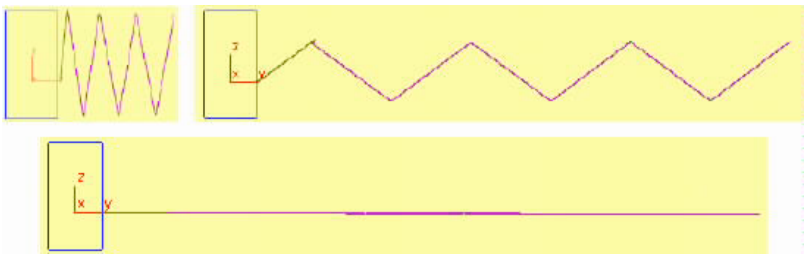

Figure 11: Shots of the solar array deployment steps

In the following four models are used. Note that all eigenmodes (em) and all frequency response modes (frm) are computed for free-free structures. For the calculation of frequency response modes all attachment forces of the respective body were taken into account. The frequency response modes are computed for all forces that act the attachment points. The models are in detail:

(1) yoke with 15 em, panels with 8 em (604)
(2) yoke with 19 em, panels with 8 em (690)
(3) yoke with 5 em + 11 frm, panels with 8 em (583)
(4) yoke with 5 em + 11 frm, panels 5 em + 13 frm (1953),

where the brackets give the necessary CPU time in seconds.

According to what was said before participation factors for free-free eigenmodes of the yoke and panels are computed for the static equilibrium phase after the jump out and after complete deployment, since these are the interesting points in time. Fig. 12 shows the simulation results for the flexible displacements of a marker in the middle of the last panel in the x directions and about the y -axis.

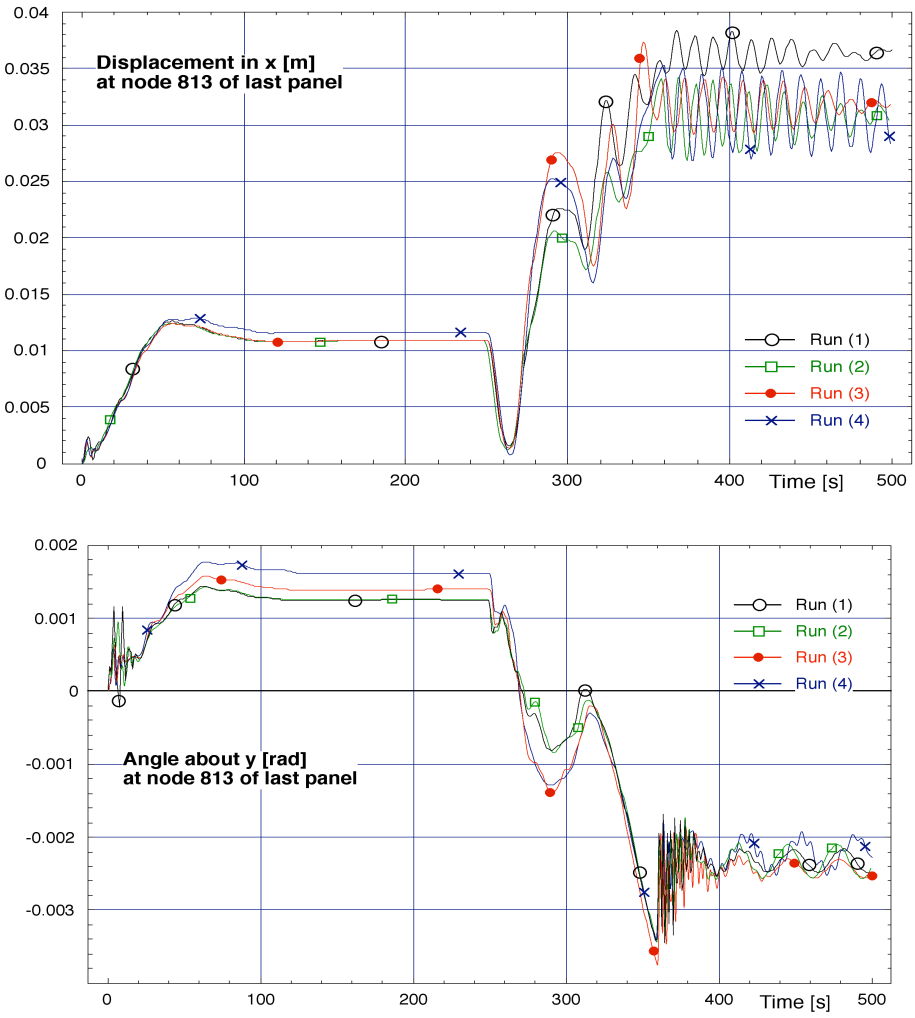

Figure 12: Displacements of the last panel

The figures above show an increasing deviation of the results for an increasing number of used frm. For the case at hand the simulation results are basically determined by two very different groups of mode shapes: the first few em are very suitable for representing the biggest part of the energy or, in other words, of the overall deformations. The frm on the other hand were computed letting $\square_0$ = 2 Hz in (27), which after making the modes orthogonal gave frequencies ranging up to 800 Hz, thus representing mostly local deformations near the attachment points. As expected, these local deformations represent only small amounts of energy with the main panel plane almost staying at rest while all little appendages and flanges are moving furiously. But it is exactly these points where the above mentioned cable loops are attached. It is therefore believed that modes that represent these special motions of the appendages give results closer to reality than other modes. With these findings the proper strategy of mode selection would be to apply participation factor methods to find say, the four

or five most important low frequency eigenmodes for the most interesting force configurations to represent the overall flexible behaviour and to use the frm method to find those modes that represent local deformations of interesting physical locations on each flexible structure. Further research on this topic is on the way.

6 CONCLUSION

This paper discusses the influence of a nonlinear formulation of flexible deformations using second order terms and presents methods for a proper selection of mode shapes for dynamical multibody analyses.

It is found that using quadratic terms to describe deformation proves beneficial if large forces are acting on slender structures that show effects of coupled tension, bending and torsion, as is the case for the example anti-roll-bar.

For extended simulations such as the deployment of a solar array in space only a modal representation of deformations is practical, giving rise to the problem of selecting proper modes. Here we propose the use of participation factor methods [4,8] to select eigenmodes for representation of the main deformations and to use frequency response modes to represent local flexible motions at the spots of interest.

REFERENCES

1 O. Wallrapp, *Nonlinear Beam Theory in Flexible Multibody Dynamics - Theory of SIMBEAM*, Intec GmbH, Wessling, Report Version March 2002.

2 O. Wallrapp and R. Schwertassek, Representation of Geometric Stiffening in Multibody System Simulation, *Int. Journal for Numerical Methods in Engineering* **32**: 1833-1850 (1991).

3 S. v. Dombrowski, Analysis of Large Flexible Body Deformation in Multibody Systems Using Absolute Coordinates, *Multibody System Dynamics* **8**: 409-432 (2002).

4 O. Wallrapp and S. Wiedemann, Simulation of Deployment of a Flexible Solar Array, *Multibody System Dynamics* **7**: 101-125 (2002).

5 R. Schwertassek, O. Wallrapp, and A. Shabana, Flexible Multibody Simulation and Choice of Shape Functions, *Nonlinear Dynamics* **20**(4): 361-380 (1999).

6 R. Schwertassek and O. Wallrapp, *Dynamik flexibler Mehrkörpersysteme*, Friedr. Vieweg Verlag, Braunschweig, 1999.

7 A. A. Shabana, Flexible Multibody Dynamics: Review of Past and Recent Developments, *Multibody System Dynamics* **1**: 189-222 (1997).

8 S. Dietz, *Vibration and Fatigue Analysis of Vehicle Systems Using Component Modes*, Berlin, Dissertation, Fortschritt-Berichte VDI, Reihe 12: Verkehrstechnik/Fahrzeugtechnik, Nr. 401, Düsseldorf, VDI-Verlag, 1999.

9 R. Schwertassek, O. Wallrapp, and S. v. Dombrowski, Modal Representation of Stress in Flexible Multibody Simulation, *Nonlinear Dynamics* **20**(4): 381-399 (1999).

10 R. Gasch, K. Knothe, *Strukturdynamik Band 2: Kontinua und ihre Diskretisierung*, Springer, 1989.